Effects of Self–Assembled Materials Prepared from V2O5 for Lithium Ion Electroinsertion

5 AUTHORS, INCLUDING:

Nelson Alexandre Galiote
University of São Paulo
6 PUBLICATIONS **62** CITATIONS

SEE PROFILE

Rodrigo Michelin Iost
University of São Paulo
23 PUBLICATIONS **252** CITATIONS

SEE PROFILE

Frank N Crespilho
University of São Paulo
64 PUBLICATIONS **1,120** CITATIONS

SEE PROFILE

Fritz Huguenin
University of São Paulo
**45** PUBLICATIONS **859** CITATIONS

SEE PROFILE

Effects of Self-Assembled Materials Prepared from V_2O_5 for Lithium Ion Electroinsertion

Nelson A. Galiote,[†] Maiuí N. L. Camargo,[†] Rodrigo M. Iost,[‡] Frank Crespilho,[‡] and Fritz Huguenin*,[†]

[†]Departamento de Química, Faculdade de Filosofia, Ciências e Letras de Ribeirão Preto, Universidade de São Paulo, 14040-901 Ribeirão Preto (SP), Brazil

[‡]Centro de Ciências Naturais e Humanas, Universidade Federal do ABC, 09210-170 Santo André (SP), Brazil

ABSTRACT: Self-assembled materials consisting of V_2O_5, polyallylamine (PAH) and silver nanoparticles (AgNPs) were obtained by the layer-by-layer (LbL) method, aiming at their application as electrodes for lithium-ion batteries and electrochromic devices. The method employed herein allowed for linear growth of visually homogeneous films composed of V_2O_5, V_2O_5/PAH, and V_2O_5/PAH/AgNP with 15 bilayers. According to the Fourier transform infrared spectra, interaction between the oxygen atom of the vanadyl group and the amino group should be responsible for the growth of these films. This interaction also enabled establishment of an electrostatic shield between the lithium ions and the sites with higher negative charge, thereby raising the ionic mobility and consequently increasing the energy storage capacity and reducing the response time. According to the site-saturation model and the electrochemical and spectroelectrochemical results, the presence of PAH in the self-assembled host matrix decreased the number of V_2O_5 electroactive sites. Thus, AgNPs were stabilized in PAH and inserted into the nanoarchitecture, so as to enhance the specific capacity. This should provide new conducting pathways and connect isolated V_2O_5 particles in the host matrix. Therefore, new nanoarchitectures for specific interactions were formed spontaneously and chosen as examples in this work, aiming to demonstrate the potentiality of the adopted self-assembled method for enhancing the charge transport rate into the host matrices. The obtained materials displayed suitable properties for use as electrodes in lithium batteries and electrochromic devices.
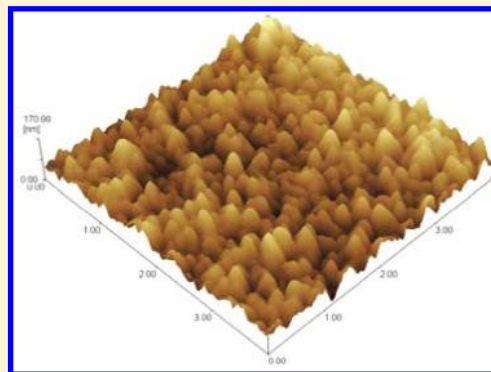
INTRODUCTION

Advances in materials science have been very important for the development of rechargeable lithium batteries and electrochromic devices. Some transition metal oxides can be employed as host matrices for the electro-insertion of lithium ions, according to the following equation

$$MO_y + xLi^+ + xe \leftrightarrows Li_xMO_y \qquad (1)$$

where M is a transition metal. Theoretically, high energy density and suitable electrochromic properties can be obtained with some of these materials. However, the rate of electrochemical reaction is normally low due to slow lithium ion diffusion into these host matrices, which culminates in energy loss and long response time for these devices.[1−5]

Considering that reactions take place in the entire volume of the materials, the use of nanomaterials is an approach for boosting the performance of these devices. In fact, the internal surface area is enhanced as compared to that of conventional oxide electrodes, and significant changes in the mass transport properties of the metal oxides are expected. Larger internal surface area can decrease the ionic diffusion pathway within the host matrices, thereby rising and diminishing the energy density of the lithium

batteries and the response time of electrochromic devices, respectively.[1,4,6,7]

Among the several kinds of nanomaterials (nanoparticles, nanowires, etc.), organic/inorganic nanocomposites can be an option for improving the electrochemical and spectroelectrochemical properties associated with lithium electroinsertion.[8,9] A route that can be used for the manufacture of these nanocomposites is the layer-by-layer (LbL) technique.[10,11] In this method, nanoarchitectures can be spontaneously formed via ionic attraction of oppositely charged materials, which allows for control of film thickness, uniformity, and composition. Moreover, the intimate contact between polymers and metal oxides can generate an electrostatic shield between the chemical species involved in the diffusion jump, which normally involves the electroinserted ions and the sites with the highest negative charge within host matrices, thereby elevating the ionic mobility and the diffusion rate.[12]

In this work, LbL nanocomposites containing V_2O_5, polyallylamine (PAH), and silver nanoparticles (AgNPs) have been prepared and investigated. V_2O_5 was chosen due to its electrochemical

and chromogenic properties, which makes it a suitable component for use as positive electrode in lithium batteries and counter electrode in electrochromic devices. This insertion electrode has a potential higher than 3 V (vs Li/Li$^+$) during the discharge process, an energy density close to 600 W·h·kg^{-1}, and a specific capacity of about 250 A·h·kg^{-1}.[13,14] These values can still be increased depending on electrode mass, rate capacities, and synthesis and deposition methods.[15] In addition, the color of this metal oxide changes from yellow to blue during lithium ion insertion. The electronic transition between bands 2pO and 3dV and the intervalence charge transfer from V^{4+} to V^{5+} are responsible for light absorption (with low molar absorptivity) in the visible range of the electromagnetic spectrum.[16]

Another important motivation for using this LbL nanocomposite was the effect of self-assembly on lithium ion diffusion. In fact, lithium ion diffusion into this host matrix is low. The lithium ion diffusion coefficient (D_{Li}) varies between 10^{-9} and 10^{-17} cm^2·s^{-1} and depends on several parameters, such as composition, preparation method, nature of the precursor, and aging time of the precursor gel.[17,18] The oxygen atoms of the vanadyl groups have a high negative charge density, and their interaction with lithium ions diminishes the ionic diffusion rate. Thus, the PAH protonated amine group can specifically and strategically adsorb onto these oxygen atoms, hence allowing for the spontaneous growth of insertion electrodes. This also gives rise to an electrostatic shield between the guest ions and the host matrices, which increases the ionic diffusion rate.

The V$_2$O$_5$ xerogel conductivity also depends on several parameters, such as the oxidation state of the vanadium ions, once this property is associated with electron hopping from the V(IV) to the V(V) sites.[19] Its value can vary between 10^{-7} and 10^0 S·cm^{-1}. Because PAH stabilizes AgNPs and allows for the formation of LbL films with polyanions in acidic medium, metallic nanoparticles can be incorporated into the V$_2$O$_5$/PAH self-assembled matrices, in order to increase the electronic conductivity and leading to high ionic diffusion rate.[20] Thus, this work shows the potentiality of the LbL method for the preparation of nanoarchitectures with suitable electrochemical and chromogenic properties for use in lithium batteries and electrochromic devices.

■ EXPERIMENTAL SECTION

V$_2$O$_5$ was synthesized following a previously described sol−gel method.[9,12,13] Briefly, 0.2 mL (4 × 10^{-4} mol) of vanadyl tris(isopropoxide), VC$_9$H$_{21}$O$_4$ (Gelest), was added to 120 mL of pure water. The volume of the obtained liquid phase was then reduced by heating the mixture under vacuum at 70 °C using a MA120 rotary evaporator over a period of ca. 4 h. This produced a yellowish solution that became a viscous, red sol−gel liquid. Commercial PAH was purchased from Aldrich. AgNPs were prepared by slow addition of an aqueous NaBH$_4$ solution (1.5 mmol·L^{-1}) to an aqueous dispersion of PAH (20 mmol·L^{-1}) and AgNO$_3$ (1.0 mmol·L^{-1}). The mixture was placed in an ice bath under stirring for 5 min, changing from colorless to yellow during the synthesis. This mixture was kept in the dark after synthesis and stockage at room temperature.

LbL films were assembled onto a fluorine doped tin-oxide (FTO) coated glass acquired from Flexitec (Curitiba, Brazil). The glass had sheet resistance ≤ 20 Ω and a geometrical area of 1 cm^2. The layers were obtained via ionic attraction of oppositely charged materials, by alternate 1 min immersions of the FTO substrate into the PAH dispersion (1.6 g·L^{-1}) in HCl solution (pH = 2) and V$_2$O$_5$ dispersion (pH = 2). After each layer deposition, the substrates were rinsed in HCl solution (pH = 2), for 30 s, and dried under nitrogen flow at room temperature. This material

will be designated Film-2 hereafter. Meanwhile, Film-3 was obtained using a similar method, by employing a mixture of AgNPs and PAH in HCl solution (pH = 2) and V$_2$O$_5$ dispersion (pH = 2).

The dip-coating technique was applied for preparation of the V$_2$O$_5$ film (Film-1). To achieve a film with high uniformity, the FTO surface was first modified by adsorption with one PAH layer, obtained by immersing FTO for one minute into the PAH dispersion, following by rinsing in HCl solution for 30 s and drying under nitrogen flow. The immersion and submersion rate was 10 mm·min^{-1}, the substrate was kept immersed into the V$_2$O$_5$ dispersion for 1 min, and the drying time was 2 min. This process was repeated, and the dip-coating films consisted of two layers.

The amount of vanadium atoms in the LbL films was determined by spectrophotometric method.[21] First, a calibration curve at 460 nm as a function of the V$_2$O$_5$ xerogel concentration (from 0.2 × 10^{-4} to 5.0 × 10^{-4} mol.L^{-1}) in 0.2 mol·L^{-1} H$_2$SO$_4$ and complexed with 3.0 × 10^{-3} mol·L^{-1} H$_2$O$_2$ was constructed. Then, this procedure was repeated with Film-1, Film-2, and Film-3, in order to determine the vanadium atoms concentration in these materials.

Film thickness was analyzed by specular reflectance using the Nanocalc 2000 program coupled with a single channel 2048 pixel CCD spectrophotometer, using a halogen lamp as the light source. The thickness values measured for Film-1, Film-2, and Film-3 were 70 ± 4 nm, 200 ± 4 nm, and 70 ± 4 nm, respectively. The geometrical area of the films was 1 cm^2. The energy dispersive spectrometry (EDS) measurements were accomplished on an IXRF (model 500 Digital Processing) spectrometer coupled to a Zeiss (model EVO 50) scanning electron microscope (SEM). Atomic force microscopy (AFM) height images were obtained on a digital Shimadzu microscope. Contact-mode AFM measurements were performed using Olympus silicon-nitride tips. The morphology and particle size were characterized using a 200 kV transmission electron microscope (TEM, model CM200; Philips). The average size of AgNPs was estimated by measuring the diameter of at least 200 particles from TEM images. Fourier transform infrared (FTIR) spectra were acquired at a resolution of 2 cm^{-1} using a BOMEN MB-102 spectrometer. The FTIR samples were deposited on a Si plate. The X-ray diffraction (XRD) of these LbL films was recorded on a Siemens D5005 diffractometer using monochromatic Cu Kα radiation. Measurements of ac electrical impedance spectroscopy were conducted between 100 and 1 kHz, at 25 °C. The LbL films were grown on a gold electrode (1 cm^2), and a dc potential of 0.0 V was applied between two gold electrodes for a symmetric cell, accomplished with 5 mV of superimposed ac amplitude.

For the electrochemical and spectroelectrochemical experiments, a platinum sheet with an area of 10 cm^2 and Ag/Ag$^+$ saturated in propylene carbonate (PC) were used as counter electrode and quasi-reference electrode, respectively. This quasi-reference electrode has a potential of 2.94 V versus Li/Li$^+$, and all potentials are referred to the Li/Li$^+$ reference electrode. A LiClO$_4$/PC electrolytic solution (0.5 mol·L^{-1}) was utilized in all the electrochemical experiments, which were carried out using an Autolab PGSTAT30 potentiostat/galvanostat. Measurements of ac electrochemical impedance spectroscopy were performed between 100 kHz and 1 mHz. Several dc potentials were accomplished with 5 mV of superimposed ac amplitude. Chromogenic analysis was performed concomitant with the electrochemical experiments using a USB4000 spectrophotometer (Ocean Optics Inc.) equipped with an LS1 tungsten halogen light source and fiber optic cables with a diameter of 600 µm. The films were placed in a cell made of optical glass, where light beams were transmitted across the film.

■ RESULTS AND DISCUSSION

Figure 1 shows the visible-near-infrared (VIS-NIR) spectrum recorded for (a) Film-1 and registered during the growth of (b) Film-2 and (c) Film-3. The band at 394 nm is attributed to
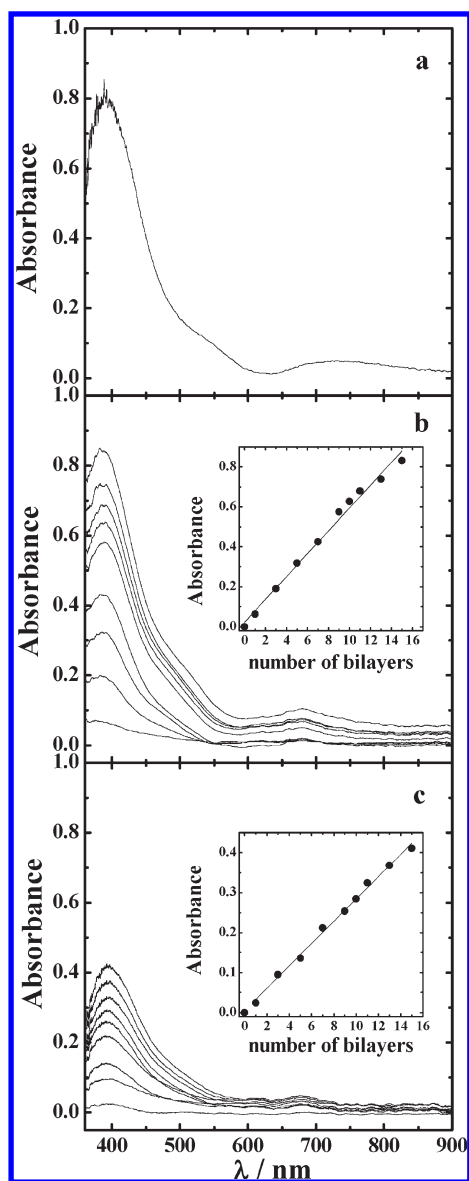
Figure 1. UV-NIR spectra obtained for (a) Film-1 and registered during the growth of (b) Film-2 and (c) Film-3. Absorbance (λ = 394 nm) as a function of the number of bilayers for Film-2 and Film-3 is shown in the inset of (b) and (c), respectively.

electronic transfer between the bands 2pO and 3dV.[16] The inset in Figure 1b,c displays the absorbance as a function of the number of bilayers at this wavelength, which indicates linear growth of the self-assembled materials and demonstrates that the self-assembly method adopted for the preparation of these materials promoted high control of film thickness and uniform V_2O_5 distribution. The average thickness of each bilayer of the self-assembled material was 13.7 and 4.6 nm for Film-2 and Film-3, respectively.

On the basis of the absorbance values obtained at 394 nm, shown in Figure 1, the amount of V_2O_5 in Film-1 and Film-2 must be similar, while the amount of this electroactive component in Film-3 must be smaller. Spectrophotometric measurements of colored complexes of vanadium and H_2O_2 were carried out in acid medium, to determine the amount of V_2O_5 in the materials (see Experimental Section), according to Almuaibed et al.[21] The molar absorptivity calculated from the absorbance

calibration curve at 460 nm as a function of vanadium concentration was 484.57 $mol^{-1} \cdot cm^{-1} \cdot L$, and the vanadium amounts were 260, 251.7, and 158 nmol in Film-1, Film-2, and Film-3, respectively. Based on these values and on the thickness of these materials, the vanadium concentration was 37×10^{-3}, 12×10^{-3}, and 22×10^{-3} $mol \cdot cm^{-3}$ in Film-1, Film-2, and Film-3, respectively.

Probably, the presence of AgNPs contributed to alterations in the charge distribution, with consequent increase in the V_2O_5 concentration during the growth of the self-assembled material. In other words, AgNPs promoted a rise in the amount of electroactive sites per bilayer. This improved the contact between V_2O_5 and the PAH chains, thereby enhancing the synergic effects associated with the electrochemical properties. Moreover, the AgNPs ensured electronic percolation into the self-assembled material. While the resistance of Film-2 augmented as a function of the number of bilayers (conductivity was close to 2.25×10^{-5} $S \cdot cm^{-1}$), the resistance of Film-3 was close to metallic resistance.

The access of lithium ions to the electroactive sites can be facilitated in the case of materials with large surface area. So morphology was investigated, and surface roughness of the films was estimated by means of atomic force microscopy. Figure 2 displays the AFM height images for (a) Film-1, (b) Film-2, and (c) Film-3 deposited on glass substrate, which reveal similar morphology for all them. It can be seen that the deposited films present holes in some regions, which can be attributed to wetting of polymeric dispersions on the glass substrate. In the hole-free regions, the smoothing surface roughness (Ra) is close to 5.47, 4.56, and 3.91 nm for (a) Film-1, (b) Film-2, and (c) Film-3, respectively. The values of Ra are close to 16.4, 18.0, and 18.4 nm for (d) Film-1, (e) Film-2, and (f) Film-3 deposited on FTO substrate, respectively. The elevation in these Ra values as compared to those determined for the films deposited on the glass substrate is associated with high FTO roughness. The Ra values of the investigated materials are close, and the difference in the electrochemical and chromogenic properties (investigated in this work) of these films should not be influenced by surface area. This difference will depend on the bulk properties of the insertion matrices, such as lithium ion mobility and the number of electroactive sites.

Figure 3a depicts the TEM image of AgNPs dispersed in PAH. These nanoparticles are spherical-like and have an effective mean diameter of ca. 5.0 nm as well as a small amount of aggregates. This suggests that PAH stabilizes the AgNPs and allows for their incorporation into the self-assembled matrix. Figure 3b corresponds to mapping of element Ag for Film-3 by EDS measurements and aims to show the distribution of AgNPs in the self-assembled materials. The AgNPs are well distributed, allowing for greater electrical connection between the V_2O_5 chains, thereby restoring the number of electroactive sites that tend to be isolated in the presence of PAH.

The XRD pattern 00l is observed for the V_2O_5 xerogel, which corresponds to ordered stacking of the V_2O_5 ribbons perpendicular to the substrate.[13] However, the presence of PAH in the materials studied in this work promoted a disordered stacking of these ribbons, as shown in Figure 4. In contrast with the diffractograms registered for Film-1 and Film-2, the diffractogram of Film-3 exhibits three diffraction peaks at 2θ values of 38°, 44°, and 64°, which are characteristic of the (111), (200), and (220) planes of the face-centered cubic structure of silver, respectively.[22] Although chloride ions are present in PAH, these results also indicate that AgCl particles are not formed in the self-assembled
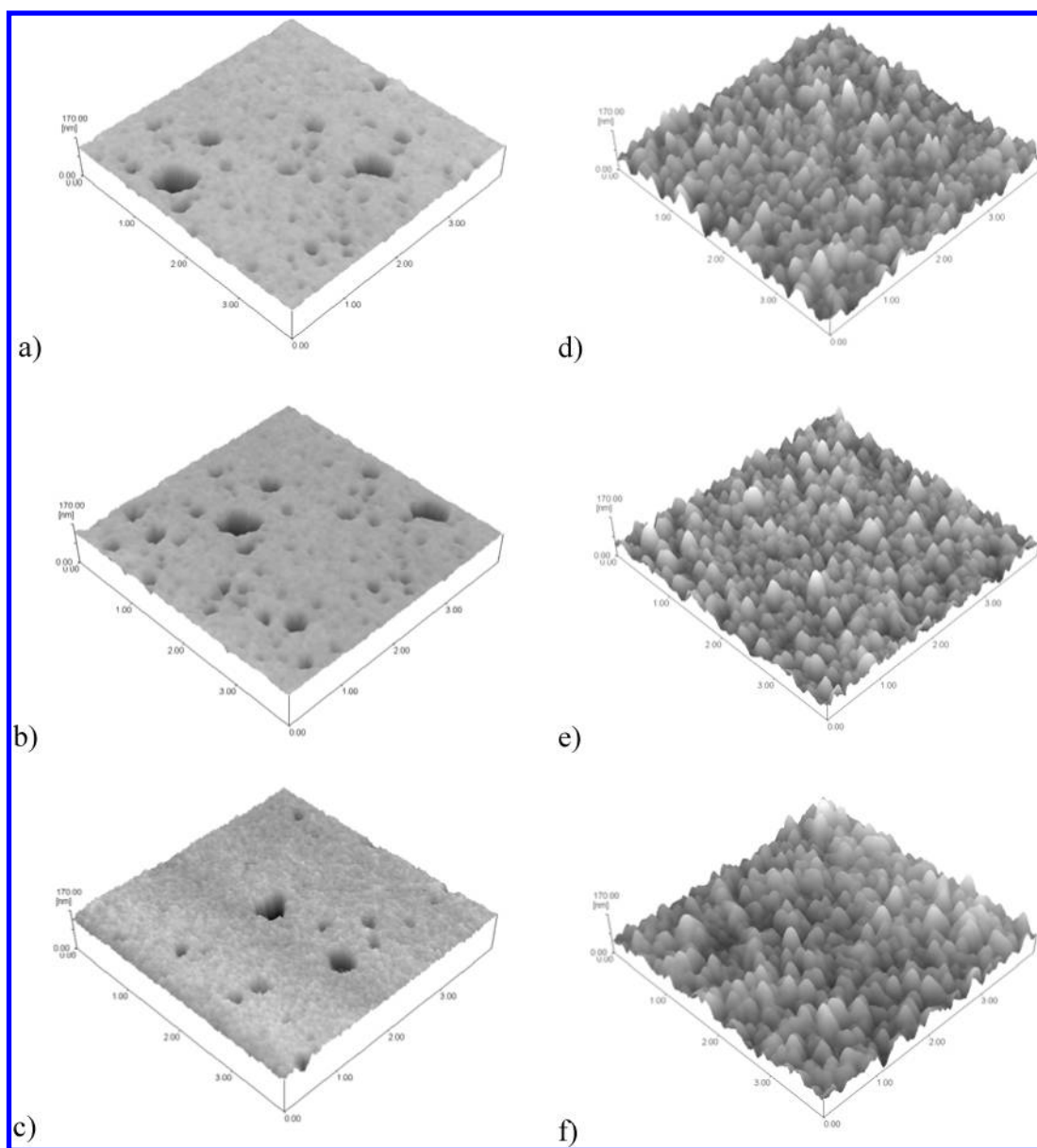
Figure 2. AFM height images of (a) Film-1, (b) Film-2, and (c) Film-3 deposited on glass substrate, and of (d) Film-1, (e) Film-2, and (f) Film-3 deposited on FTO substrate. Scanned area: 4 μm × 4 μm.

materials and that the nanoparticles observed in the TEM image really are AgNPs.

Figure 5 brings the FTIR spectra for (a) Film-1, (b) Film-2, and (c) Film-3. The bands at 495 and 751 cm^{-1} in Figure 5a are ascribed to V—O—V stretching.[23] These oxygen atoms are those positioned in the base of the VO_5 square-based pyramid, while the band associated with the vibration modes of the vanadyl group appear at 1000 cm^{-1} for Film-1. Note that the latter band shifts to 956 cm^{-1} for Film-2 and Film-3, while the other bands remain unchanged in the presence of PAH. This is an indication that the PAH amine groups preferentially interact with the oxygen atoms of the vanadyl group, independent of the presence of AgNPs in the self-assembled matrices. In fact, the electronic density on these oxygen atoms is the highest for the VO_5 square-based pyramid, and this interaction must be responsible for the growth of self-assembled materials. The band at 922 cm^{-1} in Figure 5a is also attributed to the vibration modes of the vanadyl group, in which the vanadium

ion axially coordinates with H_2O molecules. This band disappears for the self-assembled materials, suggesting that the PAH chains substitutes the H_2O molecules due to its intimate contact with the V_2O_5 chains.[23]

Figure 6 presents the chronopotentiometric curves as a function of the stoichiometric ratio between the amount of lithium ion and V_2O_5 (x in $Li_xV_2O_5$) for (a) Film-1, (b) Film-2, and (c) Film-3, respectively, at 10, 20, 50, 100, and 200 μA·cm^{-2}. The upper and lower potential limits were 4 and 2 V, respectively. These limits are normally used in the charge/discharge curves for the V_2O_5 xerogel. Insertion of lithium ions at potentials less positive than 2 V promotes a more pronounced electrochemical destabilization due to mechanical and structural changes.[24,25] Meanwhile, the upper potential employed herein is sufficient to remove the inserted lithium ions without parallel reactions with the electrolytic solution. Comparing the values of x for the three materials, it can be noted that Film-3 contains the highest
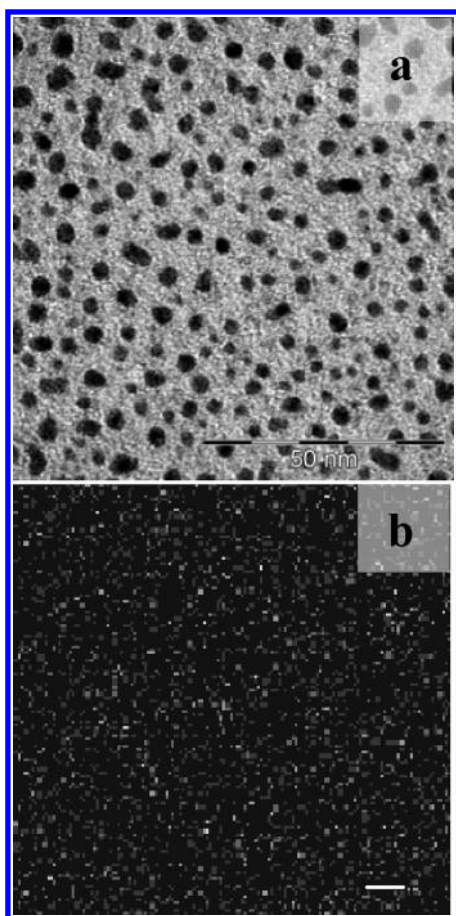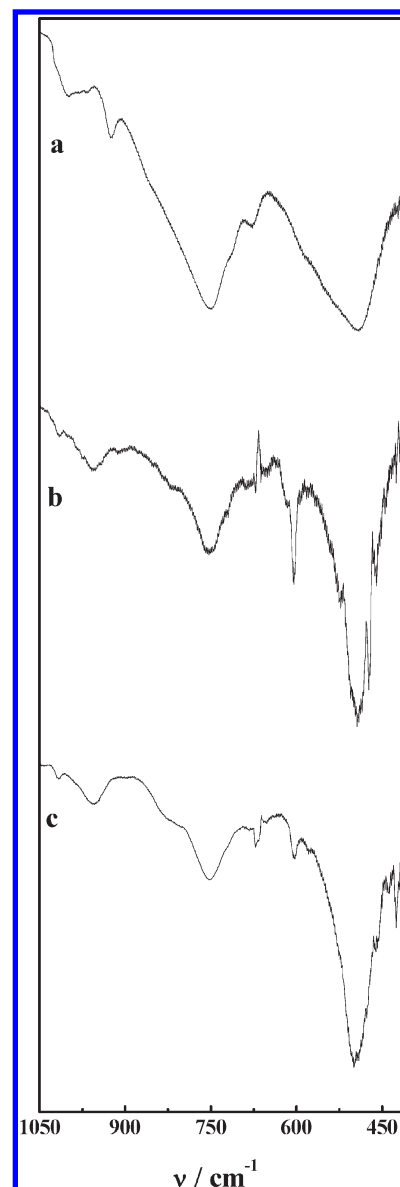
Figure 3. (a) TEM image of AgNPs dispersed in PAH. Scale bar = 50 nm. (b) EDS mapping of Ag in Film-3. Scale bar = 100 μm.
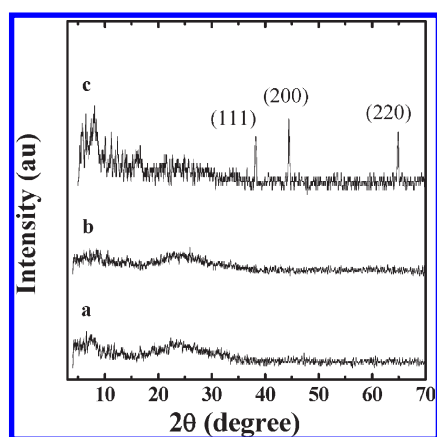
Figure 4. XRD patterns for (a) Film-1, (b) Film-2, and (c) Film-3.

**Figure 5.** FTIR spectra for (a) Film-1, (b) Film-2, and (c) Film-3.

amount of inserted lithium ion for all the applied current densities. Furthermore, it can be seen that the stoichiometric ratio x decreases with rising current density, which is probably associated with low ionic mobility and/or high charge transfer resistance (R_{ct}). During the reduction process, the values of x reduced from 0.73 to 0.51 for Film-1, from 0.53 to 0.35 for Film-2, and from 1.03 to 0.74 for Film-3 as the current density increased from 10 to 200 μA$\cdot$cm^{-2}. Meanwhile the values of x decreased from 0.68 to 0.46 for Film-1, from 0.51 to 0.33 for Film-2, and from 0.98 to 0.70 for Film-3
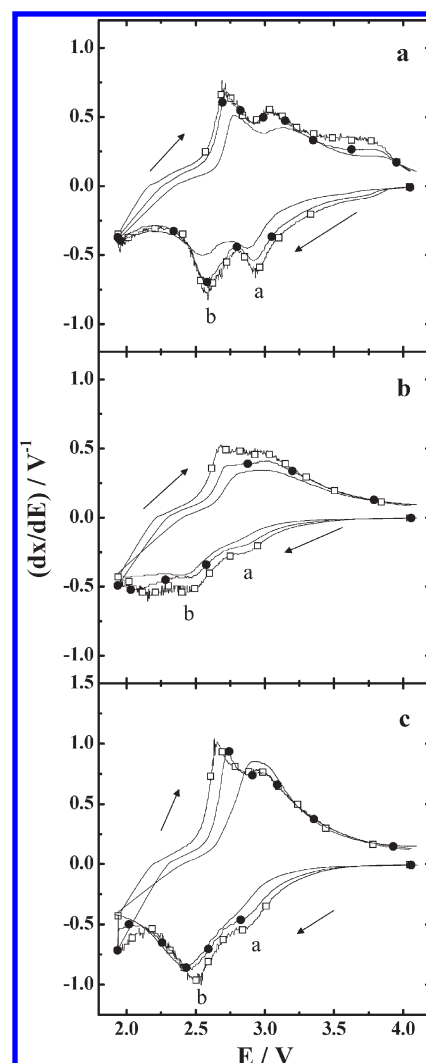
during the oxidation process. Considering the amount of electro-active material (V_2O_5), the specific capacities of Film-3 changed from 1130 C$\cdot$cm^{-3} and 157 A$\cdot$h$\cdot$kg^{-1} to 808 C$\cdot$cm^{-3} and 112 A$\cdot$h$\cdot$kg^{-1} at the lowest and highest current density applied in this work, respectively. Meanwhile, the specific capacities changed from 1307 C$\cdot$cm^{-3} and 108 A$\cdot$h$\cdot$kg^{-1} to 913 C$\cdot$cm^{-3} and 85 A$\cdot$h$\cdot$kg^{-1} for Film-1, and from 302 C$\cdot$cm^{-3} and 73 A$\cdot$h$\cdot$kg^{-1} to 233 C$\cdot$cm^{-3} and 56 A$\cdot$h$\cdot$kg^{-1} for Film-2. The factors responsible for the difference in these charge capacities will be discussed below.

Discrepancies have been found in the literature about the specific capacity values. Thus, similar experimental conditions must be considered when comparing the specific capacity values determined here with those reported in the literature. In fact, the charge storage properties depend on several experimental parameters, such as V_2O_5 mass, current density, and potential window, among others. For instance, Le et al. have shown that capacities as high as 560 A$\cdot$h$\cdot$kg^{-1} can be obtained for spin-coated V_2O_5 xerogel thin films. However, these measurements have been
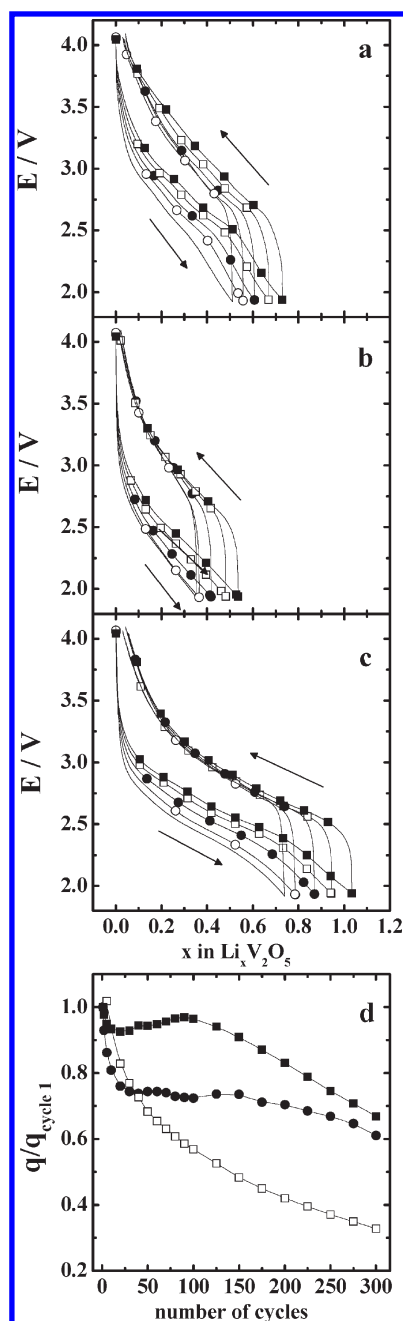
Figure 6. Chronopotentiometric curves for (a) Film-1, (b) Film-2, and (c) Film-3 at (■) 10, (□) 20, (●) 50, (○) 100, and (—) 200 μA·cm^{-2}. (d) Variation of the deinserted charge normalized by the charge obtained during the first cycle as a function of the number of cycles for (□) Film-1, (■) Film-2, and (●) Film-3. The initial oxidation charges were 7.48, 5.12, and 6.65 mC·cm^{-2} for Film-1, Film-2, and Film-3, respectively. $j = 50\ \mu$A·cm^{-2}.

Figure 7. Differential capacities (dx/dE) as a function of the potential for (a) Film-1, (b) Film-2, and (c) Film-3 at (□) 20, (●) 50, and (—) 200 μA·cm^{-2}.

conducted under the galvanostatic intermittent titration technique (GITT) regime.[26] On the other hand, Tipton et al. have determined the specific capacity of xerogel-based composite electrodes at several current densities, which decreased from ca. 200 A·h·kg^{1-} at C/100 to ca. 100 A·h·kg^{1-} at C/5 (C describes how long it takes to fully discharge the electrode).[27] In this work, high current densities for the amount of material used in the electrodes (the C rate changed from 5C to 100C) have

been applied and the capacity values for Film-3 are close to those described in the literature for similar experimental conditions.[28]

Figure 6d shows plots of the deinserted charge normalized by the charge obtained in the first cycle versus the number of cycles for Film-1, (b) Film-2, and (c) Film-3. These results demonstrate an improvement in cycling efficiency for Film-2 and Film-3 as compared to Film-1. This is evidenced by the fact that the materials composed by PAH retain more than 60% of their charge capacity after 300 cycles. In contrast, Film-1 retains about 30% of its capacity after the same number of cycles.

Figure 7 displays the differential capacities (dx/dE) as a function of the potential for (a) Film-1, (b) Film-2, and (c) Film-3 at 20, 50, and 200 μA·cm^{-2}, which were obtained from chronopotentiometric curves. There are two peaks during the lithium ion insertion for the three investigated materials, designated here as insertion sites a and b, which are positioned at more and less positive potentials, respectively. Hibino and Kudo have proposed that insertion site a is near the center of a square-planar oxygen atom and that insertion site b is around the oxygen atom of the vanadyl group.[29,30] During the reduction process at 20 μA·cm^{-2}, these insertion sites are at 2.95 and 2.60 V for Film-1, at 2.90
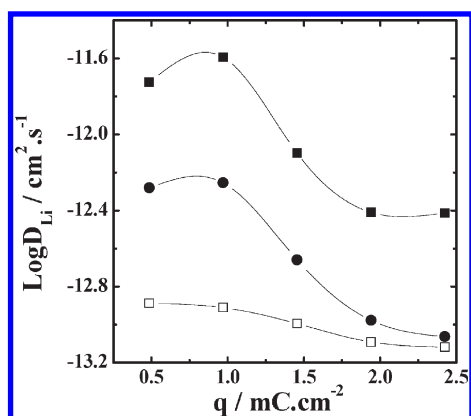
Figure 8. Logarithm of D_{Li} values as a function of the injected charge for (□) Film-1, (■) Film-2, and (●) Film-3.

and 2.45 V for Film-2, and at 2.90 and 2.50 V for Film-3. These sites are shifted to less positive potentials at higher current densities, because of low ionic mobility and high charge transfer resistance. Considering that the ratio between the current densities relative to sites *b* and *a* is higher for Film-2 and Film-3 as compared to Film-1, it can be hypothesized that the interaction between the amine group and the vanadyl group shields the interaction between the lithium ion and the vanadyl group, allowing for higher lithium ion flux in the self-assembled matrices at less positive potentials.

Aiming at better understanding the influence of PAH on the properties of lithium ions electroinserted into the host matrices, the lithium ion diffusion coefficients (D_{Li}) were determined by GITT.[31] A current with a pulse of $5\,\mu A \cdot cm^{-2}$ was applied for ca. 100 s, and the circuit was opened for 10^4 s, so that the system reached the equilibrium state. This procedure was repeated for another four times, for different injected charges, according to the equation below:[32,33]

$$D_{Li} = \frac{4}{\pi}\left[iL \frac{\left(\dfrac{dE}{dq}\right)}{\left(\dfrac{dE}{d\sqrt{t}}\right)} \right]^2 \tag{2}$$

where L is the thickness of the materials, the dE/dq term is the slope of the potential as a function of the charge (q) at the equilibrium state, and the $dE/dt^{0.5}$ term is the slope of the potential as a function of the time square root during current (i) pulses. Figure 8 represents the logarithm of the lithium ion diffusion coefficient as a function of the inserted charge for Film-1, Film-2, and Film-3. The decrease in D_{Li} values for high injected charge is attributed to the electrostatic repulsion between lithium ions.[14] Moreover, the D_{Li} values for Film-1 are lower compared to other electrodes, which can be associated with strong interaction between the lithium ion and the oxygen atom from vanadyl group. Film-2 gave the highest diffusion coefficient values, which was attributed to the electrostatic shield of this interaction due to the PAH amine group, which enhanced lithium ion mobility into the host matrix. The presence of AgNPs in the self-assembled materials diminished the D_{Li} values, which can be due to steric factors. However, these values were still higher than those achieved in the case of Film-1 and other materials consisting of V_2O_5.[18,32]
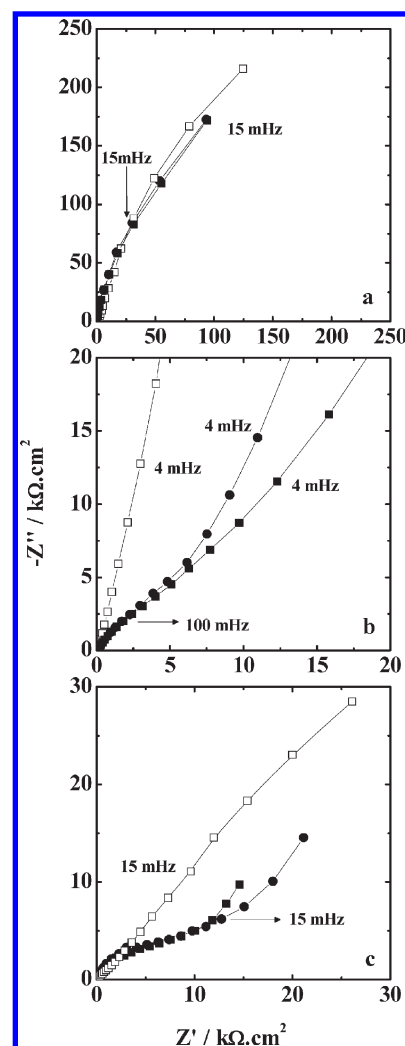
Figure 9. Nyquist diagrams for (□) Film-1, (■) Film-2, and (●) Film-3 at (a) 4.0, (b) 3.0, and (c) 2.5 V.

Figure 9 shows the Nyquist diagram for Film-1, Film-2, and Film-3 at three dc potentials: (a) 4.0 V, (b) 3.0 V, and (c) 2.5 V. The values of R_{ct} are about $390\,k\Omega \cdot cm^{-2}$ at 4.0 V for all materials, and were obtained from semicircle extrapolation to a low frequency range. These values decreased significantly for Film-1 and to $13.0\,k\Omega \cdot cm^{-2}$ for Film-2 and Film-3 at 3.0 V. These different R_{ct} values help explain the data presented in Figure 7, which evidences that access to insertion site *a* is more favorable for Film-1. These results also indicate that PAH influences in the ionic flux at the electrode/electrolytic solution interface, since the values of R_{ct} increase in the presence of PAH in the host matrices. On the other hand, AgNPs do not influence the lithium ion flux at this interface, once the impedance data associated with the charge transfer for Film-2 and Film-3 are similar. Lithium ion semi-infinite diffusion is observed for Film-1 at 2.5 V (Figure 9c), which is characterized by the straight line with a phase angle of ca. 45°. Moreover, the beginning of the semicircle observed at low frequencies is associated with trapping of charge carriers into the host matrices. As already mentioned in the literature, some materials comprise regions separated by energy barriers of different heights. Thus, the lithium ion takes longer to overcome some of the energy barriers (trapping sites) than others (diffusion sites).[7,34,35]
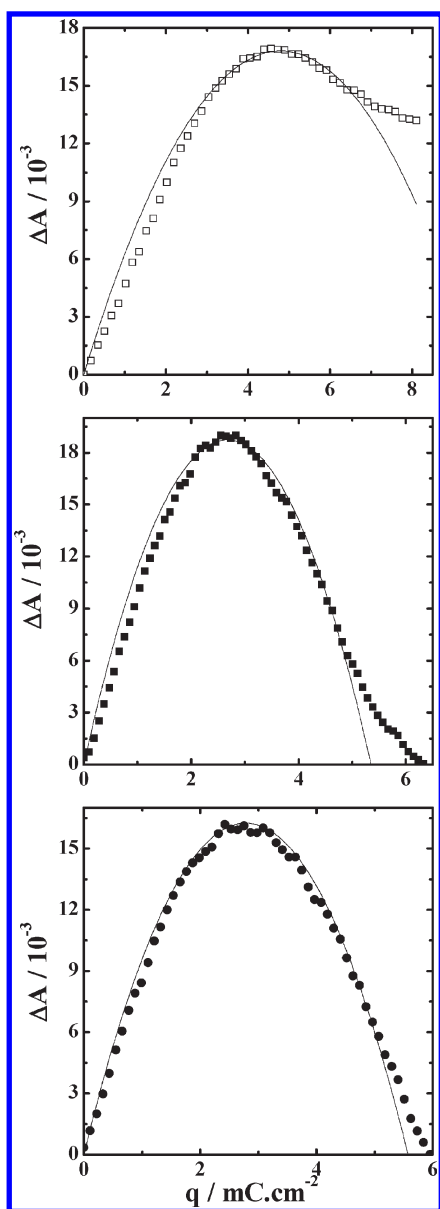
Figure 10. Absorbance change as a function of injected charge for (□) Film-1, (■) Film-2, and (●) Film-3 at $100 \ \mu A \cdot cm^{-2}$.

In the case of Film-2 and Film-3, the value of R_{ct} ($10{,}0 \ k\Omega \cdot cm^{-2}$) is still higher than that achieved for Film-1. Moreover, we can observe the lithium ion semi-infinite diffusion and a tendency for finite diffusion at the lowest frequencies, indicating a higher ionic mobility in the nanocomposites. It is also noteworthy that the trapping effect of V_2O_5 sites on lithium ions is not observed. This can be ascribed to lower interaction between the lithium ions and V_2O_5 at this potential range (insertion site b), as mentioned above.

Figure 10 displays the absorbance changes (ΔA) as a function of the injected charge for (a) Film-1, (b) Film-2, and (c) Film-3, which were obtained during the chronopotentiometric curves at $100 \ \mu A \cdot cm^{-2}$ under a monochromatic radiation of 660 nm. These absorbance changes are associated with the intervalence charge transfer from V^{4+} to V^{5+}, which can be used to determine the number of electroactive sites in these host matrices. On the

basis of the site-saturation model, these spectroelectrochemical curves can be fitted according to the following equation:[11,36]

$$\Delta A = rq\left(1 - \frac{q}{K}\right) \tag{3}$$

where r and K are positive constants. Constant r corresponds to the electrochromic efficiency for small q values ($\Delta A \approx rq$), whose values were 7.0, 14.0, and 11.9 $cm^2 \cdot C^{-1}$ for Film-1, Film-2, and Film-3, respectively. Meanwhile, constant K as divided by Faraday's constant allows for determination of the amount of electroactive sites, whose values were 99.5, 55.4, and 56.6 nmol for Film-1, Film-2, and Film-3, respectively. Considering the electroactive sites only, the stoichiometric ratio x in $Li_xV_2O_5$ is 1.7, 2.4, and 2.2 for Film-1, Film-2, and Film-3, respectively.

Although the presence of PAH increases lithium ion mobility, the amount of electroactive sites decrease due to loss of connectivity between the V_2O_5 lamellae, which probably reduces the charge capacity of Film-2 as compared to other materials. However, AgNP incorporation guarantees a better electric connection between the isolated sites of the self-assembled matrices. Hence, the charge storage capacity of Film-3 is the highest due to increased lithium ion mobility and restored number of electroactive sites.

■ CONCLUSIONS

Visually homogeneous nanocomposites grew spontaneously on conducting substrate due to interaction between the amine group of PAH and the vanadyl group of V_2O_5, which presents the highest electronic density. Considering that the interaction between the lithium ion and the vanadyl group is one of the factors responsible for low ionic mobility, energy dissipation, and long response time during electroinsertion, the employed methodology allowed for PAH adsorption in the strategic sites of the V_2O_5 host matrices, enabling shielding of this ion–dipole interaction. In fact, the values of lithium ion diffusion coefficients were higher for Film-2 and Film-3 as compared to Film-1. Moreover, no trapping effects were detected in the nanocomposites, in contrast with the electrochemical impedance data observed for Film-1. However, the presence of PAH diminished the amount of electroactive sites in V_2O_5, because of its low electronic conductivity. But this polymer ensured AgNP stability, allowing for their incorporation into the self-assembled matrices during the growth of LbL films. Electrical and spectroelectrochemical experiments showed that the AgNPs formed conducting pathways, thereby increasing the number of electroactive sites, in comparison with V_2O_5/PAH, and having higher ionic mobility, as compared to V_2O_5. In conclusion, this work suggests that nanoarchitectures with suitable properties can be spontaneously obtained, leading to better performance of lithium batteries and electrochromic devices, such as improved charge capacity and shorter response time.

■ AUTHOR INFORMATION

Corresponding Author
*E-mail: fritz@ffclrp.usp.br.

■ ACKNOWLEDGMENT

■ REFERENCES

(1) Scrosati, B.; Garche, J. *J. Power Sources* **2010**, *195*, 2419.

(2) Ellis, B. L.; Lee, K. T.; Nazar, L. F. *Chem. Mater.* **2010**, *22*, 691.

(3) Armand, M.; Tarascon, J.-M. *Nature* **2008**, *541*, 652.

(4) Aricò, A. S.; Bruce, P.; Scrosati, B.; Tarascon, J.-M.; Schalkwijk, W. V. *Nat. Mater.* **2005**, *4*, 366.

(5) Niklasson, G. A.; Granqvist, C. G. *J. Mater. Chem.* **2007**, *17*, 127.

(6) Bruce, P.; Scrosati, B.; Tarascon, J.-M. *Angew. Chem., Int. Ed.* **2008**, *47*, 2930.

(7) Facci, T.; Huguenin, F. *Langmuir* **2010**, *26*, 4489.

(8) Posudievsky, O. Y.; Kozarenko, O. A.; Dyadyun, V. S.; Jorgensen, S. W.; Spearot, J. A.; Koshechko, V. G.; Pokhodenko, V. D. *J. Power Sources* **2011**, *196*, 3331.

(9) Huguenin, F.; Nart, F. C.; Gonzalez, E. R.; Oliveira, O. N. *J. Phys. Chem. B* **2004**, *108*, 18919.

(10) Lutkenhaus, J. L.; Hammond, P. T. *Soft Mater.* **2007**, *3*, 804.

(11) Galiote, N. A.; Huguenin, F. *J. Phys. Chem. C* **2007**, *111*, 14911.

(12) Huguenin, F.; Torresi, R. M. *J. Phys. Chem. C* **2008**, *112*, 2202.

(13) Livage, J. *Chem. Mater.* **1991**, *3*, 578.

(14) Baddour, R.; Pereira-Ramos, J. P.; Messina, R.; Perichon, J. *J. Electroanal. Chem.* **1991**, *314*, 81.

(15) Chernova, N. A.; Roppolo, M.; Dillon, A. C.; Whittingham, M. S. *J. Mater. Chem.* **2009**, *19*, 2526.

(16) Bullot, J.; Cordier, P.; Gallais, O.; Gauthier, M.; Babonneau, F. *J. Non-Cryst. Solids* **1984**, *68*, 135.

(17) Holland, G. P.; Huguenin, F.; Torresi, R. M.; Buttry, D. A. *J. Electrochem. Soc.* **2003**, *150*, A721.

(18) Mège, S.; Levieux, Y.; Ansart, F.; Savariault, J. M.; Rousset, A. *J. Appl. Electrochem.* **2000**, *30*, 657.

(19) Barboux, P.; Morineau, H. E.; Livage, J. *Solid State Ionics* **1988**, *27*, 221.

(20) Xiong, C.; Aliev, A. E.; Gnade, B.; Balkus, K. L. *ACS Nano* **2008**, *2*, 293.

(21) Almuaibed, A. M.; Townshend, A. *Fresenius' Z. Anal. Chem.* **1989**, *335*, 905.

(22) Khan, M. A. M.; Kumar, S.; Ahamed, M.; Alrokayan, S. A.; AlSalhi, M. S. *Nanoscale Res. Lett.* **2011**, *6*, 1.

(23) Abello, L.; Husson, E.; Repelin, Y.; Lucazeau, G. *J. Solid State Chem.* **1985**, *56*, 379.

(24) West, K.; Zachau-Christiansen, B.; Jacobsen, T.; Skaarup, S. *Electrochim. Acta* **1993**, *38*, 1215.

(25) Huguenin, F.; Torresi, R. M. *J. Braz. Chem. Soc.* **2003**, *14*, 536.

(26) Le, D. B.; Passerini, S.; Guo, J.; Ressler, J.; Owens, B. B.; Smyrl, W. H. *J. Electrochem. Soc.* **1996**, *143*, 2099.

(27) Tipton, A. L.; Passerini, S.; Owens, B. B.; Smyrl, W. H. *J. Electrochem. Soc.* **1996**, *143*, 3473.

(28) Huguenin, F.; Torresi, R. M.; Buttry, D. A. *J. Electrochem. Soc.* **2002**, *149*, A546.

(29) Hibino, M.; Kudo, T. *Hyomen* **1998**, *36*, 45.

(30) Imamura, D.; Miyayama, M. *Solid State Ionics* **2003**, *161*, 173.

(31) Weppner, W.; Huggins, R. A. *J. Electrochem. Soc.* **1977**, *124*, 1569.

(32) Scarminio, J.; Catarini, P. R.; Urbano, A.; Gelamo, R. V.; Rouxinol, F. P.; Bica de Moraes, M. A. *J. Braz. Chem. Soc.* **2008**, *19*, 788.

(33) Rezende, A. R.; Bizeto, M. A.; Constantino, V. R. L.; Huguenin, F. *J. Phys. Chem. C* **2009**, *113*, 10868.

(34) Bisquert, J. *Electrochem. Acta* **2002**, *47*, 2435.

(35) Goodenough, J. B. In *Solid State Electrochemistry*; Bruce, P. G., Ed.; Cambridge University Press: Cambridge, 1995; p 43.

(36) Denesuk, M.; Uhlmann, D. R. *J. Electrochem. Soc.* **1996**, *143*, L186.